Notice of Retraction

G. Lv, Z. Zhang and X. Li, "Three-dimensional Electromagnetic Characteristics Analysis of Novel Linear Synchronous Motor under Lateral and Yaw Conditions of MAGLEV," in CES Transactions on Electrical Machines and Systems, vol. 6, no. 1, pp. 29-36, March 2022

After careful and considered review of the content of this article by a duly constituted expert committee, this article has been found to have violated IEEE publication principles. Specifically, this article copied content from the following sources without appropriate reference:

Masayuki Aiba; Masao Suzuki, ”Durability Verification of Combined Propulsion, Levitation and Guidance Coils” Railway Technical Research Institute Report, June 2005

Therefore, IEEE has retracted the content of this article from Xplore. When informed of the decision to retract, the authors disagreed with the retraction.

Three-dimensional Electromagnetic Characteristics Analysis of Novel Linear Synchronous Motor under Lateral and Yaw Conditions of MAGLEV

Gang Lv, *Fellow, IET*, Zhixuan Zhang, *Member*, *IEEE,* and Xiaodong Li

***Abstract*—Dynamic stability analysis of superconducting electro-dynamic maglev train under lateral and yawing motion condition is the key research content. The novel three-dimensional electromagnetic model of integrated linear synchronous motor in electro-dynamic maglev train with yawing operation condition is proposed, which can not only simultaneously achieve the propulsion, levitation and guidance performances of maglev vehicle, but also analyze the dynamic stability performance of train with yawing condition. The three-dimensional analytical method is introduced for analyzing the electromagnetic force characteristics of the linear synchronous motor with the yawing operation condition. Firstly, the topology structure and operation principle of the linear synchronous motor with yawing attitude are proposed. Secondly, the three-dimensional analytical model and expressions of electromagnetic characteristics are obtained by equivalent circuit method and Fourier decomposition method, such as levitation force, guidance force, propulsion force and yawing torque, etc. Finally, the three-dimensional electromagnetic characteristics of the linear synchronous motor are calculated under yawing operation conditions of maglev train, and the correctness of the analytical theory is verified by the finite element analysis and measured data on the test line.**

***Index Terms*—electro-dynamic maglev system, linear synchronous motor, propulsion levitation and guidance, three-dimensional electromagnetic characteristics**

I. Introduction

DUE to the advantages of large suspension height, self-stability, high system efficiency and power factor, the method of electro-dynamic suspension (EDS) has become an important research direction of transportation power development strategy [1]. The double null-flux side-wall EDS topology is gradually adopted due to its high lift-to-drag ratio and electromagnetic stiffness characteristics [2]-[5]. In the topology, the double-layer eight-shaped short circuit coils are used for levitation and guidance of maglev train; the racetrack coils installed on the side-wall guide rail are used to generate the propulsion force of the maglev train [6]-[12]. Meanwhile, there is great expectation for the low-cost implementation of ground coils which are installed along the entire length of the guideway, the linear synchronous motor(LSM) combined propulsion, levitation and guidance (PLG) is proposed [13]-[15]. The electromagnetic steady-state operation characteristics analysis of other LSM topologies has been discussed [16]-[18]. However, there is no comprehensive theory to analyze the three-dimensional (3-D) electromagnetic characteristics of the integrated LSM combined propulsion, levitation and guidance under yawing operation condition.

A novel 3-D electromagnetic characteristics model and comprehensive analysis calculation (AC) method is proposed for the novel integrated LSM with yawing condition. Firstly, the topological structure and PLG operation principle of the LSM with yawing attitude are investigated; Secondly, the analytical method of combining Fourier decomposition with equivalent circuit is proposed to analyze the 3-D electromagnetic characteristics of the LSM with yawing running condition, and the corresponding analytical expressions are obtained; Finally, based on the structure parameters of the integrated LSM used in the high-speed maglev train, the 3-D electromagnetic characteristics of the LSM are calculated under yawing operation conditions, and the correctness of the analytical expressions is verified by the finite element analysis (FEA) and experimental data.

Manuscript received January 29, 2022； revised February 13, 2022; accepted March 1, 2022. date of publication March 25, 2022; date of current version March 18, 2022.

This work was supported in part by the National Natural Science Foundation of China under Grant 52077003 and 51777009.

G. Lv and Z. Zhang are with the School of Electrical Engineering, Beijing Jiaotong University, Beijing 100044, China (e-mail: ganglv@bjtu.edu.cn, 19117037@bjtu.edu.cn).

Xiaodong Li is with the Macau University of Science and Technology,Faculty of Innovation Engineering, Macau, 999078, China.(e-mail: xdli @must.edu.mo)

(*Corresponding author: Gang Lv*)

Digital Object Identifier 10.30941/CESTEMS.2022.00005

II. The Topology Structure and Operation Principle of the LSM with Yawing Condition

A. The Topology Structure

The high-speed maglev train consists of integrated LSM combined propulsion, levitation and guidance performance, as shown in Fig. 1, where the rotation of maglev train around *z*-axis indicates yawing attitude. The integrated LSM is composed of secondary superconductivity (SC) coils and primary asymmetric combined coils. The SC coils are installed on the side of each bogie, and asymmetric combined coils are installed on the side walls on both sides of the guide rail. The asymmetric combined coils on both sides of the guide rail are connected through cable feeders, a single asymmetric combined coil is composed of two coils of the different specifications at the top and bottom through reverse connection, and the feeder point is led out from the middle reverse contact, make the front and rear in three-phase connections, and then connect them to the driving power source along the guideway.

B. The Operation Principle

The operation principle of propulsion, levitation and

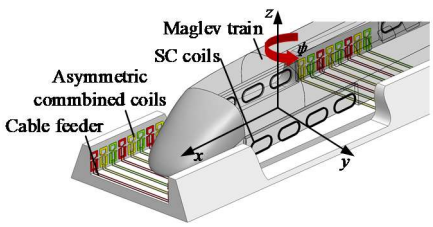

Fig. 1. The topology structure diagram of high-speed maglev train (with yawing attitude).

guidance movement of the integrated LSM with asymmetric primary structure is the same as that of the LSM with primary symmetric structure [19]-[20]. When the high-speed maglev train passes the curve or is disturbed laterally, the vehicle will show a short yaw attitude, as shown in Fig. 2. In case of the maglev train is yaw counter clockwise, the SC coils at the front side of the bogie produces the guidance force, while the SC coils at the back side produce the opposite force. Then clockwise yawing torque is generated, which ensures that the maglev train retains to the initial running condition (along the *x*-axis). (In Fig. 2, $\overrightarrow{F_y}$: guidance force; $\overrightarrow{F_x}$: propulsion force; $\overrightarrow{F_r}$: magnetic drag force; $\overrightarrow{T_\psi}$: yawing torque, ψ : yawing angle).

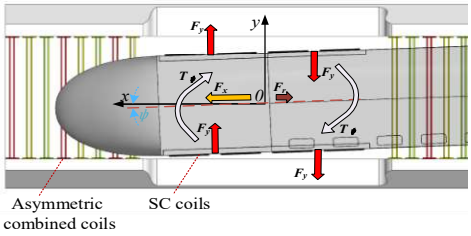

Fig. 2. The schematic diagram of yawing operation of integrated LSM (the length of the arrow indicates the peak force).

III. The 3-D Electromagnetic Characteristics Calculation of The LSM with Yaw Condition

A. The 3-D Electromagnetic Characteristics Analytical Model

The following reasonable assumptions are put forward for the integrated LSM combined PLG with yawing condition to simplify the electromagnetic theoretical calculation:

(1) The thickness of the combined coils and the SC coils is ignored; the shape of SC coils is rectangle in the electromagnetic calculation, which does not affect the running characteristics of maglev train.

(2) During normal operation of maglev train, the center of the bogie is located at the balance position and moves 5.5cm down from the center of the asymmetric combined coils, which is balanced with the gravity of the train.

(3) There is sinusoidal alternating current with constant amplitude and constant frequency in the asymmetric combined coils.

(4) The flux produced by the current of the SC coils is regarded as a constant value.

(5) When the maglev train is disturbed by lateral wind, the yaw angle of the secondary SC coils is small.

(6) The bogie, train body and guide rail are considered rigid, regardless of deflection.

(7) The electromagnetic force and torque applied to the SC coils act on the center of each coil.

The 3-D electromagnetic characteristics analytical model of the integrated LSM combined PLG with yaw condition in the high-speed maglev train is shown in Fig. 3, where U, V, W represent three-phase power supply.

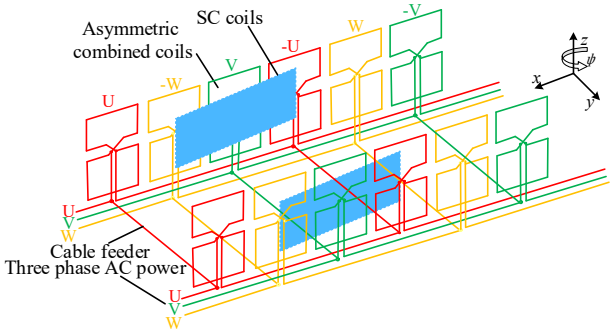

Fig. 3. The 3-D electromagnetic characteristics analytical model of the integrated LSM with yawing condition.

B. The 3-D Electromagnetic Characteristics Calculation

It is assumed that there is vertical displacement (d_z), lateral offset (d_y) and yaw counter clockwise (d_ψ) of the maglev train, as shown in Fig. 4(a). The arrangement and connection of the unit asymmetric combined coil on both sides of the guide rail is shown in Fig. 4(b). The asymmetric combined coil is composed of four coils with different sizes and inherent characteristics in the upper side and the lower side, and assuming that the induced electromotive force (EMF) of each coil is $\overrightarrow{e_{UL}}, \overrightarrow{e_{BL}}, \overrightarrow{e_{UR}}, \overrightarrow{e_{BR}}$. Where, $\overrightarrow{e_{UL}}$: EMF in the upper-left rectangular coils; $\overrightarrow{e_{BL}}$: EMF in the below-left rectangular coils; $\overrightarrow{e_{UR}}$: EMF in the upper-right rectangular coils; $\overrightarrow{e_{BR}}$: EMF in the below-right rectangular coils; and the expressions of EMF can be obtained according to Lenz's law:

$$\overrightarrow{e_{UR}} = jw\left[\phi_U + \frac{\partial \phi_U}{\partial y}(d_y + x_p d_\psi) - \frac{\partial \phi_U}{\partial x} y_0 d_\psi\right] \tag{1}$$

$$\overrightarrow{e_{BR}} = jw\left[\phi_B + \frac{\partial \phi_B}{\partial y}(d_y + x_p d_\psi) - \frac{\partial \phi_B}{\partial x} y_0 d_\psi\right] \tag{2}$$

$$\overrightarrow{e_{UL}} = jw\left[\phi_U - \frac{\partial \phi_U}{\partial y}(d_y + x_p d_\psi) + \frac{\partial \phi_U}{\partial x} y_0 d_\psi\right] \tag{3}$$

$$\overrightarrow{e_{BL}} = jw\left[\phi_B - \frac{\partial \phi_B}{\partial y}(d_y + x_p d_\psi) + \frac{\partial \phi_B}{\partial x} y_0 d_\psi\right] \tag{4}$$

$$\phi_i = \sum_{k=-\infty}^{+\infty} P_i(m)\exp(ja_k x) \qquad (i = U, B) \tag{5}$$

$$P_i = \sum_{n=1}^{+\infty} \frac{16\mu_0 N_i n_{sl} I_{sl}}{L_{sl} W_{sl}} k_l f_0(k,n) f_{1i}(k,n) \exp(-k_l y_{di}) \times \cos[a_n(d_z \pm Z_{pi})] \quad (i = U, B) \tag{6}$$

Where, x is the running distance, $x_p (p = 1,2,3,4)$ is the distance between the center of the SC coils and the center of the bogie in the running direction, y_0 is the transverse distance between the SC coils and the center of the bogie, y_{di} is the length

of air gap, Z_{pi} is the distance between upper and lower center of asymmetric combined coils, the function f_0 and f_{1i} is the shape factor of SC coils and combined coils, respectively; $n_{sl}I_{sl}$ is the magnetomotive force of SC coils, N_U and N_B is the turn number of upper and lower asymmetric combined coils, respectively; k and n is the Fourier decomposition coefficient in x-direction and z-direction, respectively; L_{sl} and W_{sl} is the Fourier decomposition period in x-direction and z-direction, respectively; a_k, a_n and k_l are expressions for k and n; μ_0 is the vacuum permeability, and $a_k = \pi k / L_{sl}$, $a_n = \pi n / W_{sl}$, $k_l = \sqrt{a_k^{\,2} + a_n^{\,2}}$, $f_0 = \dfrac{\sin(\frac{a_k l_{sl}}{2})\sin(\frac{a_n w_{sl}}{2})}{a_k a_n}$, $f_{1i} = \dfrac{\sin(\frac{a_n b_{1i}}{2})\sin(\frac{a_k a_i}{2})}{a_k a_n}$.

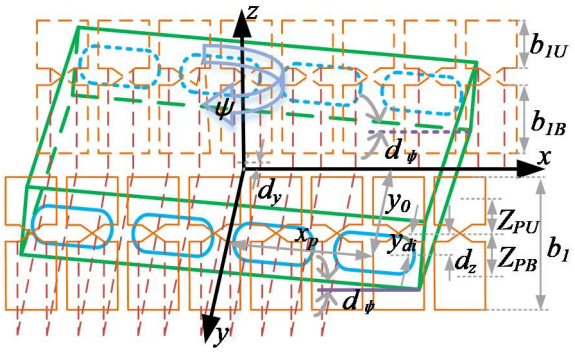

(a) Position relation diagram

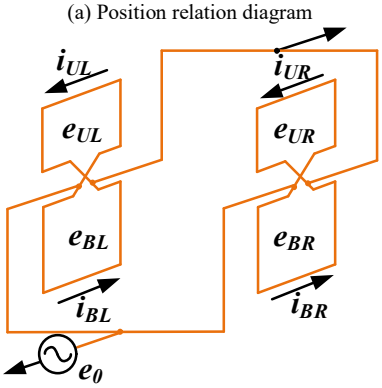

(b) Connection of unit combined coil

Fig. 4. The position relation diagram and connection of unit asymmetric combined coil.

The compound equivalent circuit diagram of the unit asymmetric combined coil is shown in Fig. 5(a), and the expressions of induced electromotive force according to Kirchhoff's voltage law and cyclic current method are as follows:

$$(R_B + jkwL_B)\overrightarrow{i_{BR}} + jkwM\overrightarrow{i_{UR}} = \overrightarrow{e_{BR}} - \overrightarrow{e_0} \quad (7)$$

$$(R_U + jkwL_U)\overrightarrow{i_{UR}} + jkwM\overrightarrow{i_{BR}} = \overrightarrow{e_{UR}} - \overrightarrow{e_0} \quad (8)$$

$$(R_B + jkwL_B)\overrightarrow{i_{BL}} + jkwM\overrightarrow{i_{UL}} = \overrightarrow{e_{BL}} - \overrightarrow{e_0} \quad (9)$$

$$(R_U + jkwL_U)\overrightarrow{i_{UL}} + jkwM\overrightarrow{i_{BL}} = \overrightarrow{e_{UL}} - \overrightarrow{e_0} \quad (10)$$

Where, R_U, R_B, L_U, L_B are the resistance and inductance of the upper and lower asymmetric combined coils; M is the mutual inductance of upper and lower asymmetric combined coils; $\overrightarrow{e_0}$ is the effective value of power supply voltage.

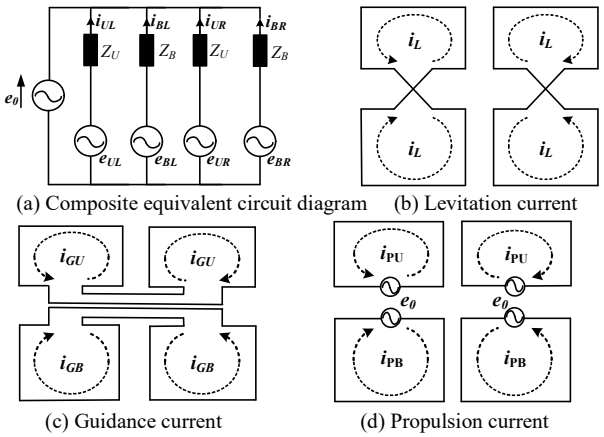

(a) Composite equivalent circuit diagram (b) Levitation current

(c) Guidance current (d) Propulsion current

Fig. 5. The composite equivalent circuit and current decomposition of unit asymmetric combined coil

The current of each branch can be decomposed into the levitation current ($\overrightarrow{i_L}$), guidance current (the upper rectangular coils: $\overrightarrow{i_{GU}}$; the below rectangular coils: $\overrightarrow{i_{GB}}$) and propulsion current (the upper rectangular coils: $\overrightarrow{i_{PU}}$; the below rectangular coils: $\overrightarrow{i_{PB}}$) by solving the expression (7-10), as shown in Fig.5 (b)-(d), and the current expressions of each coil according to Kirchhoff's current law are as follows:

$$\overrightarrow{i_{BR}} = \overrightarrow{i_L} + \overrightarrow{i_{GB}} + \overrightarrow{i_{PB}}$$

$$= \frac{(R_U + jkwL_U)\overrightarrow{e_{BR}} - jkwM\overrightarrow{e_{UR}} - Z_U'\overrightarrow{e_0}}{Z_2} \quad (11)$$

$$\overrightarrow{i_{UR}} = -\overrightarrow{i_L} + \overrightarrow{i_{GU}} + \overrightarrow{i_{PU}}$$

$$= \frac{-jkwM\overrightarrow{e_{BR}} + (R_B + jkwL_B)\overrightarrow{e_{UR}} - Z_B'\overrightarrow{e_0}}{Z_2} \quad (12)$$

$$\overrightarrow{i_{BL}} = \overrightarrow{i_L} - \overrightarrow{i_{GB}} + \overrightarrow{i_{PB}}$$

$$= \frac{(R_U + jkwL_U)\overrightarrow{e_{BL}} - jkwM\overrightarrow{e_{UL}} - Z_U'\overrightarrow{e_0}}{Z_2} \quad (13)$$

$$\overrightarrow{i_{UL}} = -\overrightarrow{i_L} - \overrightarrow{i_{GU}} + \overrightarrow{i_{PU}}$$

$$= \frac{-jkwM\overrightarrow{e_{BL}} + (R_B + jkwL_B)\overrightarrow{e_{UL}} - Z_B'\overrightarrow{e_0}}{Z_2} \quad (14)$$

Where, $Z_U' = R_U + jkwL_U - jkwM$ (15)

$$Z_B' = R_B + jkwL_B - jkwM \quad (16)$$

$$Z_U = R_U + jkwL_U \quad (17)$$

$$Z_B = R_B + jkwL_B \quad (18)$$

$$Z_1 = Z_U' + Z_B' \quad (19)$$

$$Z_2 = Z_U Z_B + (kwM)^2 \quad (20)$$

The expressions of levitation current, guidance current and propulsion current can be obtained by solving expressions (11-14):

$$\overrightarrow{i_L} = \sum_{k=-\infty}^{+\infty} \frac{jkw}{Z_1} P_1 \exp(ja_k x) \quad (21)$$

$$\overrightarrow{i_{GU}} = \sum_{k=-\infty}^{+\infty} -\overrightarrow{i_{G1}} + \frac{Z_B{}'}{Z_1}\overrightarrow{i_{G2}} \tag{22}$$

$$\overrightarrow{i_{GB}} = \sum_{k=-\infty}^{+\infty} \overrightarrow{i_{G1}} + \frac{Z_U{}'}{Z_1}\overrightarrow{i_{G2}} \tag{23}$$

$$\overrightarrow{i_{PU}} = \sum_{k=-\infty}^{+\infty} \frac{Z_B{}'}{Z_1}\overrightarrow{i_P} \tag{24}$$

$$\overrightarrow{i_{PB}} = \sum_{k=-\infty}^{+\infty} \frac{Z_U{}'}{Z_1}\overrightarrow{i_P} \tag{25}$$

Where, $P_1 = P_B - P_U$ (26)

$$P_2 = Z_U{}' P_B + Z_B{}' P_U \tag{27}$$

$$\overrightarrow{i_{Gi}} = \sum_{k=-\infty}^{+\infty} \frac{jkw}{Z_i}\left(\frac{\partial P_i}{\partial y}dy + \frac{\partial P_i}{\partial \psi}d\psi\right)\exp(ja_k x) \quad (i=1,2) \tag{28}$$

$$\overrightarrow{i_P} = \sum_{k=-\infty}^{\infty} \frac{jkwP_2\exp(ja_k x) - Z_1\overrightarrow{e_0}}{Z_2} \tag{29}$$

$$P_{ij} = \frac{\partial P_i}{\partial j} \qquad (i=1,2, \quad j=y,\psi) \tag{30}$$

The voltage balance equation of one phase can be obtained by formula (29):

$$\overrightarrow{e_0} = \sum_{k=-\infty}^{\infty} \frac{-Z_2\overrightarrow{i_P}}{Z_1} + \frac{jkwP_2\exp(ja_k x)}{Z_1} \tag{31}$$

In the formula, the first item is the impedance voltage drop of the LSM, and the second item is the motional EMF of the LSM. In addition, the fundamental component of the motional EMF is as follows:

$$\overrightarrow{E_0} = \frac{2w}{\left|Z_1(1)\right|^2}\left|Z_1^*(1)P_2(1)\right|\sin(wt-\beta) \tag{32}$$

$$\tan\beta = \frac{\mathrm{Im}(Z_1^*(1)P_2(1))}{\mathrm{Re}(Z_1^*(1)P_2(1))} \tag{33}$$

Where, * is conjugate sign, (1) is k=1 in the corresponding formulas. Here, compared with the differential component of the magnetic field produced by the SC coils, the phase of the motional EMF shifts by an angle β.

The levitation force ($\overrightarrow{F_{zz}}$ and $\overrightarrow{F_{zp}}$), guidance force ($\overrightarrow{F_y}$), propulsion force ($\overrightarrow{F_x}$), magnetic drag force ($\overrightarrow{F_r}$) and yawing torque ($\overrightarrow{T_\psi}$) are obtained based on equations (21-25):

Levitation force produced by levitation current in asymmetric combined coils:

$$\overrightarrow{F_{zz}} = L_p\,\mathrm{Re}[\overrightarrow{i_L}\frac{d\phi_1^*}{dz}] = L_p\sum_{k=-\infty}^{\infty}\frac{jkw}{Z_1}P_1P_{1z} \tag{34}$$

Where, $L_p = \tau / l_c$; τ is the pitch of SC coils and l_c is the pitch of the asymmetric combined coils.

Levitation force produced by propulsion current in asymmetric combined coils:

$$\begin{aligned}\overrightarrow{F_{zp}} &= 2L_p\,\mathrm{Re}[\overrightarrow{i_{PU}}\frac{d\phi^*{}_U}{dz} + \overrightarrow{i_{PB}}\frac{d\phi^*{}_B}{dz}] \\ &= \frac{L_p\overrightarrow{i_p}}{2\left|Z_1(1)\right|^2}[\mathrm{Im}(Z_1^*(1)P_{2z}(1))\cos(wt) - \mathrm{Re}(Z_1^*(1)P_{2z}(1))\sin(wt)]\end{aligned} \tag{35}$$

Guidance force produced by guidance current in asymmetric combined coils:

$$\overrightarrow{F_y} = L_p\,\mathrm{Re}[\overrightarrow{i_{GU}}\frac{d\phi^*{}_U}{dy} + \overrightarrow{i_{GB}}\frac{d\phi^*{}_B}{dy}] = L_p\sum_{k=-\infty}^{\infty}\frac{jkw}{Z_1}(P_1P_{1y} + \frac{P_{2y}{}^2}{Z_2}dy) \tag{36}$$

Propulsion force produced by propulsion current in asymmetric combined coils:

$$\begin{aligned}\overrightarrow{F_x} &= 2L_p\,\mathrm{Re}[\overrightarrow{i_{PU}}\frac{d\phi^*{}_U}{dx} + \overrightarrow{i_{PB}}\frac{d\phi^*{}_B}{dx}] \\ &= \frac{L_p\overrightarrow{i_P}a_k(1)}{2\left|Z_1(1)\right|^2}[\mathrm{Re}(Z_1(1)P_2(1))\cos(wt) + \mathrm{Im}(Z_1(1)P_2(1))\sin(wt)]\end{aligned} \tag{37}$$

Magnetic drag force produced by the current of each branch in asymmetric combined coils:

$$\begin{aligned}\overrightarrow{F_r} &= L_p\,\mathrm{Re}[\overrightarrow{i_{UR}}\frac{d\phi^*{}_U}{dx} + \overrightarrow{i_{BR}}\frac{d\phi^*{}_B}{dx} + \overrightarrow{i_{UL}}\frac{d\phi^*{}_U}{dx} + \overrightarrow{i_{BL}}\frac{d\phi^*{}_B}{dx}] \\ &= \frac{-2a_k wL_pP_1^2}{Z_1}\end{aligned} \tag{38}$$

Yawing torque produced by the yaw current in asymmetric combined coils:

$$\begin{aligned}\overrightarrow{T_\psi} &= L_p\,\mathrm{Re}[\overrightarrow{i_{GU}}\frac{d\phi_U{}^*}{d\psi} + \overrightarrow{i_{GB}}\frac{d\phi_B{}^*}{d\psi}] \\ &= L_p\sum_{k=-\infty}^{\infty}\frac{jkw}{Z_1}(P_1P_{1\psi} + \frac{P_{2\psi}{}^2}{Z_2}d\psi)\end{aligned} \tag{39}$$

The power factor of the integrated LSM is obtained based on equation (31):

$$p.f. = \cos(\phi) = \frac{1}{\{1+[\frac{X_{ph}(\left|\overrightarrow{V_{ph}}\right| - \left|\overrightarrow{E_{ph}}\right|\cos\delta) - R_{ph}\left|\overrightarrow{E_{ph}}\right|\sin\delta}{R_{ph}(\left|\overrightarrow{V_{ph}}\right| - \left|\overrightarrow{E_{ph}}\right|\cos\delta) + X_{ph}\left|\overrightarrow{E_{ph}}\right|\sin\delta}]^2\}^{1/2}} \tag{40}$$

Where, $R_{ph} = \frac{n_b R_U R_B}{2(R_U+R_B)}$; $X_{ph} = \frac{n_b\left[L_UL_B + M(L_B+L_U)\right]}{2(L_U+L_B)}$;

$\overrightarrow{E_{ph}} = \frac{n_m}{4}(\overrightarrow{e_{UL}} + \overrightarrow{e_{BL}} + \overrightarrow{e_{UR}} + \overrightarrow{e_{BR}})$; $\overrightarrow{V_{ph}} = n_m\overrightarrow{e_0}$; n_m: number of asymmetric combined coils coupling with SC coils; n_b: total number of combined coils; ϕ: power factor angle; δ: power angle.

The efficiency of the integrated LSM is obtained based on equation (31):

$$\eta = \frac{\left|\vec{E}_{ph}\right|}{\left|\vec{V}_{ph}\right|}\frac{R_{ph}(-\left|\vec{E}_{ph}\right| + \left|\vec{V}_{ph}\right|\cos\delta) + X_{ph}\left|\vec{V}_{ph}\right|\sin\delta}{R_{ph}(\left|\vec{V}_{ph}\right| - \left|\vec{E}_{ph}\right|\cos\delta) + X_{ph}\left|\vec{E}_{ph}\right|\sin\delta} \tag{41}$$

IV. The 3-D Electromagnetic Characteristics Analysis by AC, FEA, and Experimental Verification of the LSM

In order to verify the correctness of the 3-D electromagnetic analysis calculation model of the LSM with yawing operation condition, the structure parameters and circuit parameters of the LSM in the high-speed maglev train are adopted, as shown in

Table I and Table II. Here, the section length ratio is taken as 12 in one feeder section of the partitioned control. The 3-D electromagnetic force characteristics and propulsion characteristic curve of the LSM with yawing operation condition are calculated and compared with the FEA results obtained by ANSYS 19.2. The FEA model and experimental test coils of the LSM are shown in Fig. 6. Specifically, the 3-D FEA model consists of two parts: primary combined coils laid along the ground and secondary on-board SC coils. The secondary SC coils is surrounded by the moving region-band. Meanwhile, the 3-D finite-element method is one of the more powerful numerical techniques for solving Maxwell's field equations. For given boundary conditions and specified system geometry, one is able to obtain sufficient information for a system by using 3-D finite-element computer codes. The calculation process of 3-D finite-element method is: (1) mesh element subdivision; (2) linear interpolation; (3) unit analysis; (4) overall stiffness matrix synthesis; (5) solving linear equations.

TABLE I
The structure parameters of one LSM [14]

Primary coils	value	Secondary coils	value
Primary length (m)	10.8	Secondary length (m)	5.4
Primary width (m)	0.76	Secondary width (m)	0.50
Number of coils	48	Number of coils	8
Polar distance (m)	0.45	Polar distance (m)	1.35
Coil length (m)	0.355	Coil length (m)	1.07
Upper Coil width (m)	0.235	Coil width (m)	0.50
Upper Coil width (m)	0.375	Turns	1400
Turns	24	Air gap length (m)	0.195
Distance between Up and Down coil (m)	0.08	Bogie quality (kg)	20000
		Yaw inertia (kgm^2)	56680

TABLE II
The circuit parameters of one LSM

Primary combined coil	value	Secondary coil	value
Upper resistance (R_U/ mΩ)	12.23	Resistance (R_{SC})	0
Lower resistance (R_B/ mΩ)	12.93	Self-inductance (L_{sc}/H)	2.02
Upper-inductance (L_U/mH)	0.24	Nominal voltage(kV)	33
Lower-inductance (L_B/mH)	0.36	Operation current (I_{sl}/A)	500
Mutual inductance between upper and lower coil (L_{FR}/ μH)	0.37	Power angle (deg.)	40
Propulsion current (A)	390	Sync-speed (m/s)	135
Frequency (f/Hz)	50	Temperature (K)	<20

A. The 3-D Electromagnetic Force and Torque of the LSM

The variation curves of 3-D electromagnetic force and yaw torque of the LSM with different lateral offset distances and yawing angles are shown in Fig. 7. The variation law of levitation force under different yawing angles and different lateral offset conditions is shown in Fig. 7(a). The levitation force increases slowly with the increase of lateral offset when the yaw angle is small, which is mainly caused by the increase of magnetic field change rate in the vertical direction. When the yaw angle is too large, the change rate of the vertical magnetic field in the left and right air gaps is roughly the same, and the

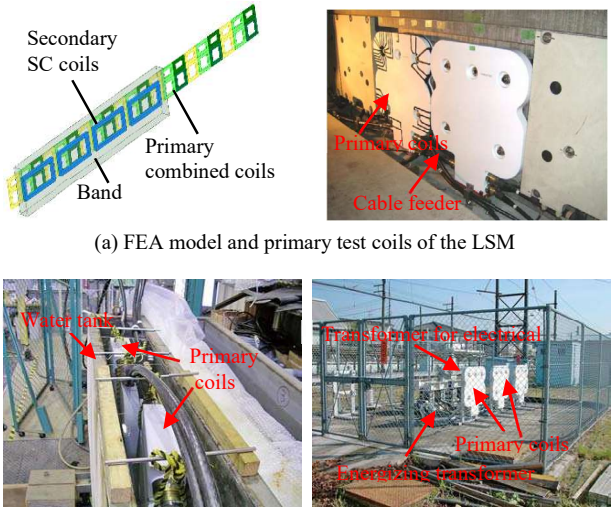

(a) FEA model and primary test coils of the LSM

(b) Test device for long term outdoor test

Fig. 6. The FEA model and test coils of the LSM in high-speed maglev train [21]-[22].

levitation force is basically unchanged. The variation law of guidance force under different yawing angles and different lateral offset conditions is shown in Fig. 7(b). With the increase of the right deviation distance of the train, the lateral guidance force produced by the LSM increases gradually, so as to ensure that the train can return to the lateral balanced position. With the increase of yawing angle, the guidance force increases rapidly, which is mainly caused by the large magnetic field change rate in the transverse direction under yawing conditions. Due to the small coupling between guidance and yawing, the relationship between the change of guidance force and transverse deflection distance is not linear. The variation law of magnetic drag force under different yawing angles and different lateral offset conditions is shown in Fig. 7(c). The magnetic drag force is basically not affected by the variation of transverse deviation distance and yawing angle, mainly due to the variation of magnetic field in bilateral air gap of the LSM is almost zero. The variation law of yawing torque under different yawing angles and different lateral offset conditions is shown in Fig. 7(d). The yawing torque increases gradually with the increases of lateral offset distance and with the increase of yawing angle. Moreover, the change rate of yaw torque decreases with the increase of yaw angle. The 3-D AC results are comparable to the FEA results, which proves the rationality of the above analysis.

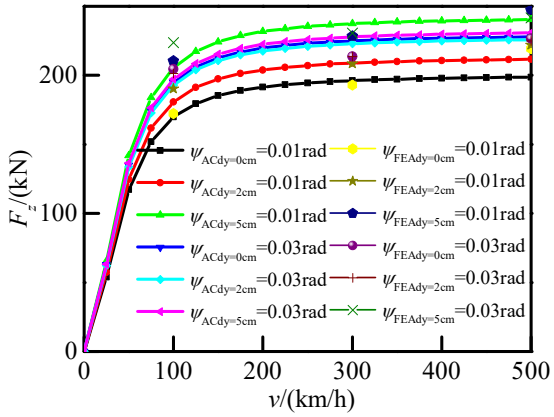

(a) Levitation force of AC and FEA

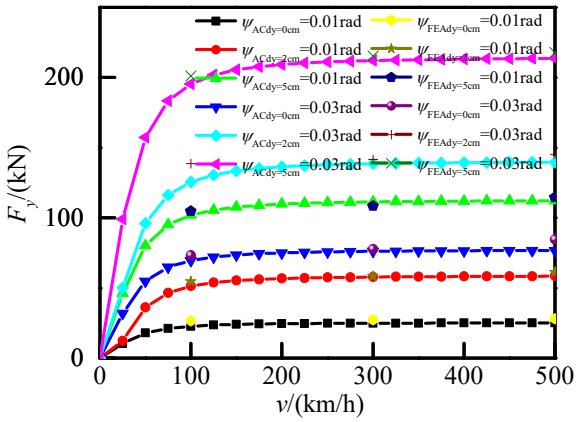

(b) Guidance force of AC and FEA

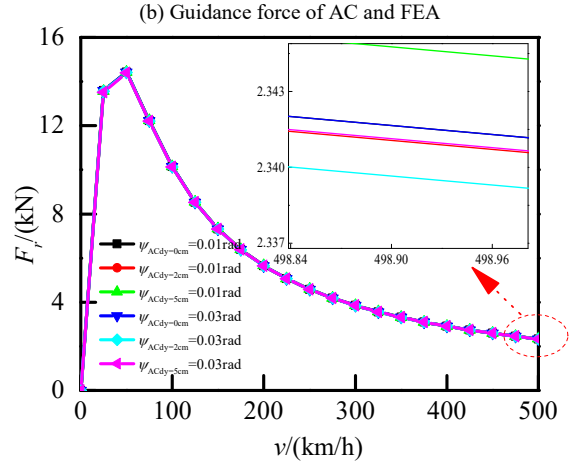

(c) Magnetic drag force of AC

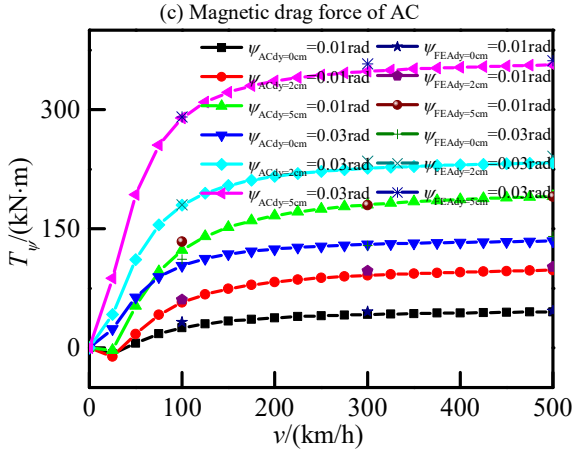

(d) Yaw torque of AC and FEA

Fig. 7. The variation curve of 3-D electromagnetic force and torque with different lateral offsets (*dy*) and yawing angles (ψ).

B. The Propulsion Characteristics Curve of the LSM

The variation curves about the propulsion force, power factor and efficiency at different power angles of the LSM with different lateral offsets and yawing angles are shown in Fig.8. The change of yawing angle and lateral offset basically has no effect on the power factor and efficiency of the LSM. On the contrary, the peak value of propulsion force increases with the increase of lateral offset and yawing angle, which is mainly caused by the inconsistent change of air gap magnetic density on both sides of the LSM. The power factor, efficiency and propulsion force increase first, then decrease with the increase of power angle. The peak value of propulsion force is the largest when the power angle is near 90 degrees.

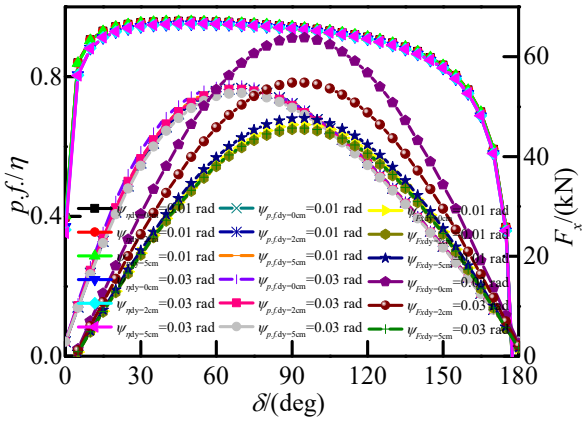

Fig. 8. The variation curve of propulsion characteristics with different lateral offsets (*dy*) and yawing angles (ψ).

C. The 3-D Electromagnetic Characteristics Experimental Verification of the LSM

To confirm the characteristics of the LSM, the electromagnetic forces are measured by the measurement combined coils temporarily installed at the maglev test line. The force in three directions (longitudinal, lateral and vertical) at the same time are measured when the coil was set at the guideway sidewall on the load converters. In order to decrease test error, magnetic forces at primary coils are derived from sum of or difference between magnetic forces as two lateral opposed primary coils. To reduce the influence of sympathetic vibration of the primary coils and load cells, after integrating these values with the time, the forces are obtained as follows:

$$F_{si} = \frac{v}{l_c}\int (F_{sri} + F_{sli})dt \qquad (i = x, y, z) \tag{42}$$

where, F_{si} is the forces on primary coils; F_{sri} is the forces at right primary coils; F_{sli} is the forces at left primary coils [23]. In addition, the guidance stiffness is derived from the difference between guidance forces.

The comparison between the AC and experimental results about the lift-to-drag ratio (ratio of levitation force to magnetic drag force), guidance stiffness (ratio of guidance force per unit lateral displacement) and propulsion force of the LSM are shown in Fig. 9 [24]. Compared with the data of experiment, the error of the AC is 5.72%, 6.10%, 1.73% and 5.69% respectively. It can be concluded from the above 3-D electromagnetic performance results that the error range between the AC and the FEA, experimental data are less than 10%, and the error is within the acceptable range, the validity of the 3-D electromagnetic characteristics analytical model of the LSM is verified. When the speed of the LSM is slightly higher than the take-off speed, the dynamic stability of the LSM is poor. Multiple measuring points can accurately reflect the electromagnetic force performance of the LSM at low speed. With the velocity increase of the LSM, the dynamic stability of the EDS maglev vehicle is enhanced, and fewer measurement points can also accurately reflect the PLG performance of the LSM. The experimental error mainly come from three aspects: (1) In the test, measurement of forces on a differential ground coil is affected by a differential vehicle fluctuation and coil

irregularity, primary current for lateral displacement and yaw angle error are relatively large; (2) In the test, the lateral distance between the SC coils and the combined coils will be changed due to the increase of the coil insulation thickness; (3) In the test, the force sensor will produce eddy current when the SC coils in maglev train passes through, resulting in inevitable measurement error.

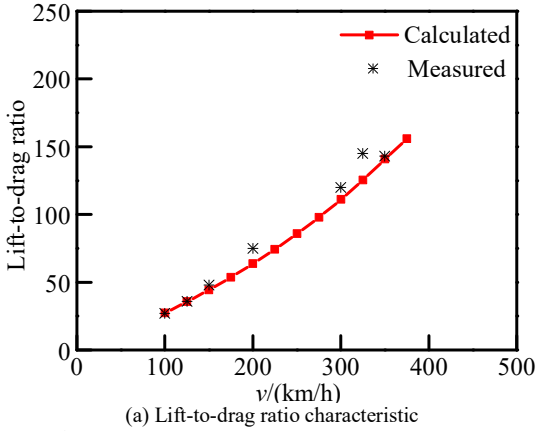

(a) Lift-to-drag ratio characteristic

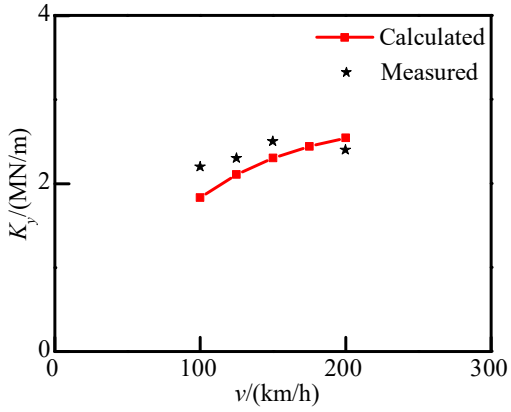

(b) Guidance stiffness characteristic

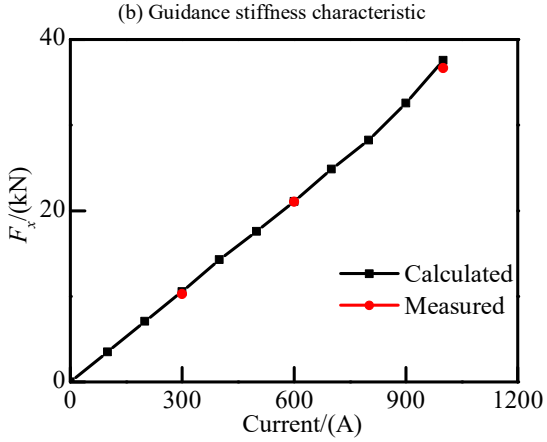

(c) Propulsion characteristic

Fig. 9. The 3-D electromagnetic characteristics of the LSM between the AC and experiment.

V. Conclusion

In the manuscript, the 3-D electromagnetic characteristic of the novel LSM for EDS high-speed maglev train with yaw attitude are analyzed. Firstly, the 3-D electromagnetic analytical model of the LSM with yawing attitude is investigated, and the 3-D characteristics calculation expressions of the LSM are obtained, such as propulsion force, levitation force and stiffness, guidance force and stiffness, yaw torque and stiffness, power factor and efficiency. Finally, the 3-D electromagnetic characteristics of the LSM are calculated under yawing operation conditions, and the correctness of the analytical expressions is verified by the FEA and test. The following main conclusions are obtained: (1) During the operation of high-speed maglev train, there is small electromagnetic coupling characteristic between the guidance condition and yawing condition; (2) The yawing attitude has little effect on the power factor and efficiency of the LSM, while significantly affect the guidance and propulsion force; (3) The error of 3-D electromagnetic performance results between the AC and the FEA, experimental data are less than 10%; (4) When the yaw and lateral fault condition occurs, the lift-to-drag ratio change of LSM is small, the guidance force and propulsion force increases with the increases of yaw angle, which indicate that the LSM has certain self-stability characteristics.

References

[1] L. Hao, Z. Huang, F. Dong, D. Qiu, B. Shen and Z. Jin, "Study on Electrodynamic Suspension System with High-Temperature Superconducting Magnets for a High-Speed Maglev Train," *IEEE Transactions on Applied Superconductivity*, vol. 29, no. 2, pp. 3600105, 2019.

[2] E. E. Burkhardt, J. Schwartz, and S. Nakamae, "Analysis of superconducting magnet (SCM)-ground coil interactions for EDS Maglev coil configurations," *IEEE Transactions on Applied Superconductivity*, vol. 3, no. 1, pp. 430-433, 1993.

[3] T. Wahana, "Study of superconducting magnetic suspension and guidance characteristics on loop tracks," *IEEE Transactions on Magnetics*, vol. 11, no. 6, pp. 1704-1711, 2003.

[4] S. Fujiwara, "Characteristics of EDS magnetic levitation with ground coils for levitation arranged on the side wall," *Electrical Engineering in Japan*, vol. 108, no. 3, pp. 101-110, 1988.

[5] P. L. Ribani, N. Urbano, "Study on Figure-Eight-Shaped Coil Electrodynamic Suspension Magnetic Levitation Systems Without Cross-Connection," *IEEE Transactions on Magnetics*, vol. 36, no. 1, pp. 358-365, 2000.

[6] G. Lv, Y. Liu, T. Zhou and Z. Zhang, "Analysis of Suspension and Guidance System of EDS Maglev Based on A Novel Magnetomotive Force Model," in *IEEE Journal of Emerging and Selected Topics in Power Electronics*, 2020, doi: 10.1109/ JESTPE.2020.3029802.

[7] S. Fujiwara, T. Fujimoto, "Characteristics of combined levitation and guidance eds maglev system," *Electrical Engineering in Japan*, vol. 113, no. 3, pp. 123-134, 1993.

[8] T. Gong, G. Ma, et al., "Calculation and Optimization of Propulsion Force of a Real-Scale REBCO Magnet for EDS Train," in *IEEE Transactions on Applied Superconductivity*, vol. 29, no. 5, pp. 1-6, Aug. 2019.

[9] S. Ohashi, "Equivalent Model of the Side Wall Electrodynamic Suspension System," *Electrical engineering in Japan*, vol. 124, no. 2, pp. 63-76, 1998.

[10] Y. Cai, G. Ma, Y. Wang, et al, "Semi-analytical Calculation of Superconducting Electrodynamic Suspension Train Using Figure-Eight-Shaped Ground Coil," *IEEE Transactions on Applied Superconductivity*, vol. 30, no. 5, pp. 3602509, 2020.

[11] Z. Y. Guo, J. Li, D. F. Zhou, "Study of a Null-Flux Coil Electrodynamic Suspension Structure for Evacuated Tube Transportation," *Symmetry*, vol. 11, no. 10, pp. 1239-, 2019.

[12] T. Yonezu, K. Watanabe, E. Suzuki and T. Sasakawa, "Study on Electromagnetic Force Characteristics Acting on Levitation/Guidance Coils of a Superconducting Maglev Vehicle System," *IEEE Transactions on Magnetics*, vol. 53, no. 11, pp. 8300605-, 2017.

[13] J. Fujie, "An Advanced Arrangement of the Combined Propulsion, Levitation and Guidance System of Superconducting Maglev," *IEEE Transactions on Magnetics*, vol. 35, no.5, pp. 4049-4051, 1999.

[14] T. Fujimoto, T. Murai, M. Suzuki, "Development of Propulsion, Levitation and Guidance Coils in EDS Maglev," *Proceedings of the Maglev 2000* (The 16th International Conference on Magnetically Levitated System and Linear Drives), 2000-6.

[15] J. L. He, H. T. Coffey, D. M. Rote, "Analysis of the combined Maglev levitation, propulsion, and guidance system," *IEEE Transactions on Magnetics*, vol. 31, no. 2, pp. 981-987, 1995.

[16] K. Liu et al., "Experimental and numerical studies of a linear synchronous motor with the secondary made of coated superconductor," *CES Transactions on Electrical Machines and Systems*, vol. 3, no. 3, pp. 297-301, 2019.

[17] Z. Wang, J. W. Zhao, L. J. Wang, M. Li and Y. P. Hu, "Combined Vector Resonant and Active Disturbance Rejection Control for PMSLM Current Harmonic Suppression," *IEEE Transactions on Industrial Informatics*, vol. 16, no. 9, pp. 5691-5702, Sept. 2020.

[18] W. Rui, M. Xu, P. Guo and J. Xu, "Improved study on position measurement system for linear motor applied in electromagnetic launch system," *CES Transactions on Electrical Machines and Systems*, vol. 3, no. 2, pp. 216-220, 2019.

[19] G. Lv, Z. Zhang, Y. Liu and T. Zhou, "Characteristics Analysis of Linear Synchronous Motor Integrated with Propulsion, Levitation and Guidance in High-speed Maglev System," *IEEE Transactions on Transportation Electrification*, vol. 7, no. 4, pp. 3185-3193, 2021.

[20] G. Lv, Z. Zhang, Y. Liu and T. Zhou, "Analysis of Forces in Linear Synchronous Motor with Propulsion, Levitation and Guidance for High-speed Maglev," in *IEEE Journal of Emerging and Selected Topics in Power Electronics*, doi: 10.1109/JESTPE.2021.3065459.

[21] N. Maki, H. Okuda, T. Tatsumi, et al, "A combined system of propulsion and guidance by linear synchronous motors," *IEEE Transactions on Power Apparatus & Systems*, vol. 96, no. 4, pp. 1109-1116, 1977.

[22] Aiba. M, Ota. S and Suzuki M, "浮上式鉄道用推進コイルの絶縁性能を評価する," *超電導技術の鉄道応用*, vol. 74, no. 8, pp. 24-27, August 2017.

[23] T. Murai, T. Fujimoto and S. Fujiwara, "Test run of combined propulsion, levitation and guidance system at Miyazaki test track," *IEEJ Transactions on Industry Applications*, vol. 115, no. 9, pp. 1165-1172, 1995.

[24] M. Aiba, T. Murai, M. Suzuki, N. Takahashi, K. Yoshikawa, "Development of the Ground Coil for Practical Use by the Combined Propulsion, Levitation and Guidance System," *Proceeding of Maglev 2004*, pp. 849-855, 2004.

Gang Lv (M'15) received the Ph.D. degree in electric machine and driven from Beijing Jiaotong Univ., Beijing, China, in 2007.

From 2007 to 2009, he was a Postdoctoral Research Fellow with the Technology Center, CRRC Qingdao Sifang Locomotive and Rolling Stock Co.Ltd., Qingdao, China. In 2007, he joined Sch. of E.E., Beijing Jiaotong Univ., where he is currently a Professor. His research interests include analysis and control of linear machines.

Prof. Lv is a Fellow of the Institution of Engineering and Technology. He has served as chair and organizing committee member for many international conferences. He is a managing director of the Electric Drive Technology Sub-Committee - Electric Vehicle Technical Committee- IEEE PES China.

Zhixuan Zhang received the B.Eng. degree in electrical engineering from Shanxi Univ., Shanxi, China, in 2016.
He is currently working toward the Ph.D. degree in electric machine and driven in Beijing Jiaotong Univ., China, where he has been engaged in the design and analysis of linear synchronous machines.

Xiaodong Li (Senior Member, IEEE) received the B.Eng. degree in electrical engineering from Shanghai Jiao Tong University, Shanghai, China, in 1994, and the M.A.Sc. and Ph.D. degrees in electrical engineering from the University of Victoria, Victoria, BC, Canada, in 2004 and 2009, respectively.

From 1994 to 2002, he was an Electrical Engineer with HongWan Diesel Power Corporation, Zhuhai, China, where he conducted maintenance of the diesel power generation system. In 2009, he joined the Faculty of Information Technology, Macau University of Science and Technology, Macau, China, where he is currently an Associate Professor. He has authored or coauthored more than 50 papers in international conference proceedings and journals and holds four U.S. patents and five Australia Innovation patents. His research interests include high-frequency power converters and its applications.

Dr. Li received the IEEE Power and Energy Society Best Paper Prize in 2007 and the Bank of China Research Excellence Award from the Macau University of Science and Technology in 2013.